Minimum Conduction Loss ZVS Control for Buck-Type Active Filter Operating as Decoupling Circuit

Behnam Koushki, Praveen Jain, Alireza Bakhshai
Department of Electrical and Computer Engineering
Queen's University
Kingston ON, Canada
11fbk@queensu.ca

***Abstract*— It is becoming a useful and favorable trend to remove unreliable E-caps from the single-phase AC-DC converters which are being widely used in renewable energy applications and energy storage systems, without letting the low frequency power penetrating into the DC-side. Active filter is an attractive solution for this. Since active filter processes a major part of power, its performance affects the performance of the converter. Therefore, it is important that it operates efficiently for a wide range of operation. A minimum conduction loss ZVS control is proposed for buck-type active filter, which can be used across the DC-link of two-stage converters or across the DC side of the single-stage AC-DC converters. The control minimize the conduction losses for the buck active filter as well as obtaining ZVS for all the switching instants. Loss comparison with hard-switched control and other ZVS control methods are presented and show the effectiveness of the proposed method. Simulation and experimental results are presented.**

Keywords—ZVS; Variable frequency control; Decoupling circuit; E-Cap less; AC-DC Converter; Active filter; Minimum Conduction Loss Control;

I. INTRODUCTION

In many renewable energy applications such as wind, solar or fuel cell, or in many energy storage systems, the power from the renewable or energy storage DC-side transfers to the single-phase AC grid. One of the options is a two-stage topology with an intermediate DC-link. In this configuration, there is an AC-DC front-end inverter or PFC between the grid and DC-link and another DC-DC converter which is placed between the DC-link and DC source [1]. The other option is using a single-stage AC-DC topology [2, 3]. The low frequency power ripple with the frequency of two times of the grid frequency is a bi-product of single-phase AC-DC power conversion. In two-stage topologies, this power is partly or mostly absorbed by the DC-link capacitor. In single-phase topology, this power is transferred to the DC side. In two-stage topologies, a large capacitor is needed to have the power mostly absorbed with a small ripple. Therefore, a large bulky Electrolytic Capacitor or in short E-cap should be used which decreases the reliably of the system. Passage of the low frequency power ripple to the DC-source is not favorable as some of the renewable sources need to work with constant DC current and voltage [4, 5]. In the case of an energy storage system, low frequency ripple causes extra heat production, micro cycle to the battery and these reduce the lifespan of the battery [6].

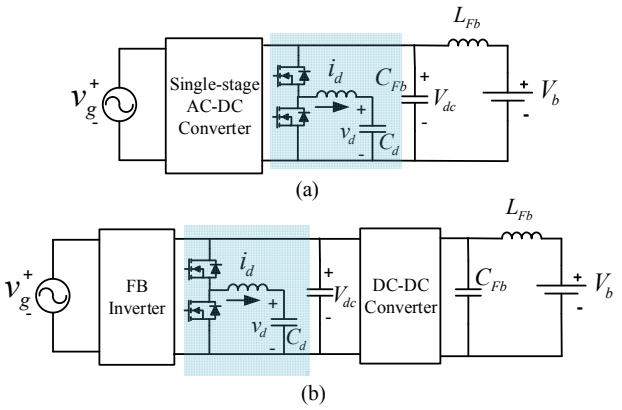

Fig. 1. Use of active filter in (a) single-stage AC-DC converter and (b) two-stage AC-DC converter as decoupling circuit.

One solution to avoid low frequency power from going to battery and remove the unreliable E-cap at the same time is to use DC-link with large ripple [7]. With this solution, the variable DC-link voltage makes the inverter and DC-DC controller more complicated in addition to imposing extra voltage stress to the DC-link connected components. The better solution is using an active filter. This solution downsizes the capacitor as well as absorbs the power ripple completely without adding extra voltage stress. Therefore, reliable Film capacitors can be used instead [5].

The active filter can be added to the DC-link of two stage such as [8] or at the DC source terminal in single stage topologies [4, 9 and 10]. The active filter can be a bi-directional buck [11], boost or buck-boost converter [12, 13].

The active filter circuit though is a simple DC-DC converter, since it operates with a time varying output voltage, under different input voltage and peak power without a load, its control and design can be challenging. The efficiency of active filter is important as it process the reactive power, which is as large as

the power transferred to the load of the AC-DC converter. Different control techniques have been proposed to obtain a good performance in terms of efficiency and dynamic for active filter circuit. In [10] a ZVS control is proposed to eliminate switching loss while wide range of operation and a controller is designed to obtain proper dynamic operation. In [11] a DCM control with fixed switching frequency operation is presented to have ZCS for the turn off of the switches. The high peak current due to CCM operation can cause higher conduction loss in this method.

Here, a variable frequency minimum conduction loss ZVS control (VF-MCL-ZVS control) for the buck-type active filter is presented. The control ensues ZVS for all the switching instants and minimum conduction loss for the wide-range of operation. ZVS together with the minimum conduction loss operations ensures the optimal performance of the active filter. Analysis and derivations are given. The design for wide range of DC-voltage and peak power is given. The proposed control method is compared with the ones of hard switching CCM control and ZVS CCM method presented in [10, 9]. Simulation and experimental results are provided to confirm the theory.

II. Proposed Control and Analisys

Active filter used for absorbing the AC low frequency power ripple is referred as "decoupling circuit" as well. Fig.1 shows the application of buck-type decoupling circuit at two different AC-DC topologies. In most of the applications such as EV battery charger in which DC voltage varies between 200-400 depending on the state of the charge of the battery, the AC-DC converter operates with variable output DC voltage,V_b. Also peak power, P_m, is variable. In two-stage topologies, the DC-link voltage, V_{dc}, can also vary when V_b varies to obtain better performance [14]. Therefore, in both single-stage and two-stage applications, the decoupling circuit should be controlled in such a way that for all the operating points (P_m, V_{dc}) the proper performance is achieved.

If grid voltage, v_g, is shown in (1) and power transferred, p_t, is shown in (2), the desired decoupling voltage, v_d, can be calculated from (3) as was shown in [10].

$$v_g = V_m \cos(\omega_g t) \tag{1}$$

$$p_t = P_m \cos(2\omega_g t + \theta_g) + P_m \cos(\theta_g) \tag{2}$$

$$v_d = \sqrt{{V_0}^2 + (P_m/C_d\omega_g)(\sin(2\omega_g t + \theta_g) - \sin(\theta_g))} \tag{3}$$

Assuming that d_d, the duty cycle of the upper switch of the buck converter, is being controlled so that decoupling voltage, v_d, follow desired reference shown in (3). Fig.2 shows the operation of the decoupling circuit at a specific operating point over one line cycle. Since the d_d is known at each switching cycle, by controlling the f, ripple is controlled so that it is large enough just to obtain ZVS for valley and peak times during each switching cycle. These two times are the switching times as shown in Fig.2.

This control makes sure that ZVS exist with the price of minimum possible ripple to obtain that. This minimum ripple current, Δi_d, is shown in (4).

$$\Delta i_d = \begin{cases} 2(i_{d,av} - i_\varepsilon) & i_{d,av} > 0 \\ 2(i_{d,av} + i_\varepsilon) & i_{d,av} < 0 \end{cases} \tag{4}$$

i_ε is the minimum current needed to charge and discharge snubber capacitances across the MOSFETs and is a function of battery voltage. It is shown in (5). In this equation, t_{qMin} is the dead time and should be smaller than 10% of the minimum of $(1 - d_d T)$ and $d_d T$. Since the proposed VF-MCL-ZVS is a type of CCM with a variable frequency, CCM equations for CCM can be applied. Form the ripple current equation, the frequency as a function of Δi_d can be calculated from (6).

$$i_\varepsilon = \frac{2C_s V_b}{t_{qMin}} \tag{5}$$

$$f = \frac{1}{L_d \Delta i_d} \frac{v_{dec}}{V_b} (V_b - v_{dec}) \tag{6}$$

Replacing Δi_d form (4) and neglecting i_ε compared to $i_{d,av}$ yields the equation for f.

$$f = \frac{1}{2L_d |i_{d,av}|} \frac{v_{dec}}{V_b} (V_b - v_{dec}) \tag{7}$$

As it is shown in Fig.2 when $i_{d,av}$ approaches zero, f goes to infinity to limit the ripple. However in reality there is an upper

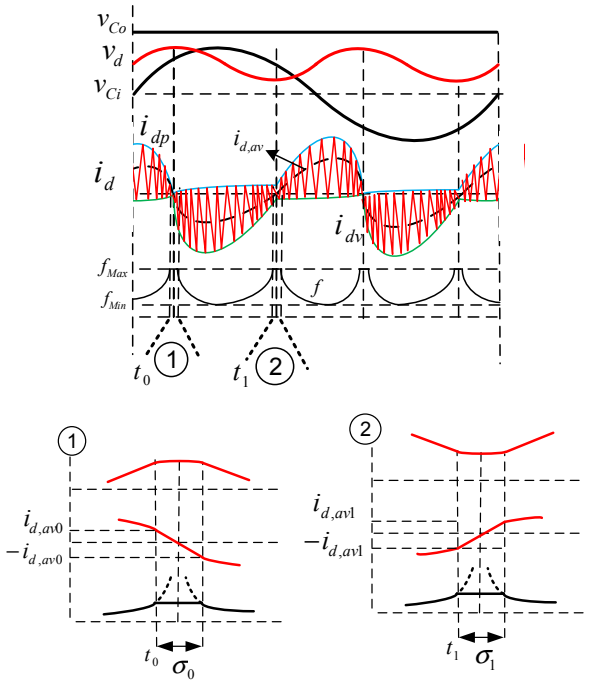

Fig. 2. Basic waveforms of proposed control method.

limitation set for frequency, f_{Max}. When frequency reaches there, it stays at this frequency for the duration σ shown in Fig.2 within this period, the ripple can go higher than (4) which is the optimum ripple needed while ZVS is still maintained. It is also possible that ripple remains not enough for ZVS and therefore hard switching happens within this small window. The decoupling circuit should be designed so that this window remains small and usually below 10% of the whole line cycle. Since the proposed VF-MCL-ZVS is a type of CCM with a variable frequency, CCM equations of the buck converter in CCM mode can be applied. Form the ripple current equation, the frequency as a function of Δi_d can be calculated from (8).

$$f = \frac{1}{L_d \Delta i_d} \frac{v_{dec}}{V_b} (V_b - v_{dec}) \tag{8}$$

Replacing Δi_d form (4)(7) and neglecting i_ε compared to $i_{d,av}$ yields the equation for f.

$$f = \frac{1}{2L_d |i_{d,av}|} \frac{v_{dec}}{V_b} (V_b - v_{dec}) \tag{9}$$

The minimum of the frequency over one line cycle, f_{Min}, depends on L_d. Therefore, f_{Min} should be calculated before the design. As shown in Fig.2(b), f_{Min} happens somewhere close to either valley or peak of $i_{d,av}$. It can be proven mathematically that when $i_{d,av}$ reaches its extremums, i_{davExt} (its valley and peak), f reaches f_{Min}. Therefore f_{Min} can be calculated from (10).

$$f_{Min} = \frac{1}{2L_d |i_{davExt}|} \frac{v_{dec0}}{V_b} (V_b - v_{dec0}) \tag{10}$$

In this equation, v_{dec0} is the value of v_{dec} when i_{davExt} happens. The extremums $i_{d,av}$ happen when (11) happens. The value of extremum of $i_{d,av}$ is calculated and is shown in (12) again. The value of v_{dec} at this time can be calculated form (13).

$$\sin(2\omega_g t_0 + \theta_g) = (\sqrt{V_0^2 - 1} - V_0) \tag{11}$$

$$\begin{aligned} i_{davExt} &= C_d \frac{x'}{2\sqrt{x}} \\ &= \mp C_d \omega_g \sqrt{\frac{P_m}{C_d\, \omega_g} \frac{2\left(1 - V_0^2 + V_0\sqrt{V_0^2 - 1}\right)}{\sqrt{V_0^2 - 1}}} \end{aligned} \tag{12}$$

$$v_{dec0} = \sqrt{\frac{P_m}{C_d\, \omega_g} \sqrt{V_0^2 - 1}} \tag{13}$$

Replacing from (11) and (13) in (10) yields the minimum frequency and is shown in (14).

$$f_{Min} = \frac{\sqrt{V_0^2 - 1}}{2L_d C_d \omega_g \sqrt{2\left(1 - V_0^2 + V_0\sqrt{V_0^2 - 1}\right)}} \left(1 - \frac{1}{V_b} \sqrt{\frac{P_m}{C_d\, \omega_g} \sqrt{V_0^2 - 1}} \right) \tag{14}$$

Another equation needed for the design of L_d is the relationship between f_{Max} and σ. This window is small. As it is shown in Fig.2, the moment f reaches f_{Max}, is either t_0 or t_1. The value of decoupling current at these times are $i_{d,av,0}$ and $i_{d,av,1}$respectively. It can be assumed that v_{dec} is almost equal to $v_{dec,Max}$ at t_0 and is equal to $v_{dec,Min}$ at t_1. The duration of the window starting with t_0 during which f is kept constant and equal to f_{Max} is σ_0 and similarly the duration of the window starting with t_1 during which f is kept constant and equal to f_{Max} is σ_1. These window durations are small and they happen around the peak and valley of v_{dec}. For the σ_0 window, with the assumption that v_{dec} remains constant and equal to $v_{dec,Max}$, $i_{d,av,0}$ can be calculated form (15).

$$i_{d,av,0} = \frac{1}{2L_d f_{Max}} \frac{v_{dec,Max}}{V_b} (V_b - v_{dec,Max}) \tag{15}$$

To approximate the σ_0, the linear approximation of $i_{d,av}$ around the $v_{dec,Max}$ and $i_{d,av} = 0$ is used. Equation (16) use this approximation to relate σ_0 to other parameters.

$$\sigma_0 = 2\frac{i_{d,av,0}}{\frac{di_{d,av}}{dt}|_{t\,=\,t_{Max}}} = 2\frac{i_{d,av,0}}{C_d \frac{d^2 v_d}{dt^2}|_{t\,=\,t_{Max}}} \tag{16}$$

Replacing $i_{d,av,0}$ from (15) and v_d from (3) into (16) yields:

$$\sigma_0 = \frac{(1 + V_0)}{2V_b L_d f_{Max} C_d} \frac{(V_b - \sqrt{\mathrm{A}(1 + V_0)})}{{\omega_g}^2} \tag{17}$$

In which A is a parameter shown in (18). For the σ_1 similar calculation, can be done. $i_{d,av,1}$ which is the current at the time t_1 can be calculated from (18) and σ_1 can be calculated form (20).

$$A = \frac{P_m}{C_d \omega_g} \tag{18}$$

$$i_{d,av,1} = \frac{1}{2L_d f_{Max}} \frac{v_{dec,Min}}{V_b} (V_b - v_{dec,Min}) \tag{19}$$

$$\sigma_1 = \frac{(1 - V_0)}{2V_b L_d f_{Max} C_d} \frac{(V_b - \sqrt{A(1 - V_0)})}{{\omega_g}^2} \tag{20}$$

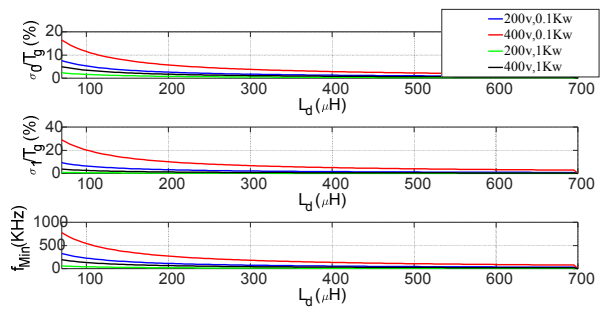

Fig. 3. Inductor design for VF-MCL-ZVS: , f_{Min} and σ_i plotted for 4 marginal different operating points.

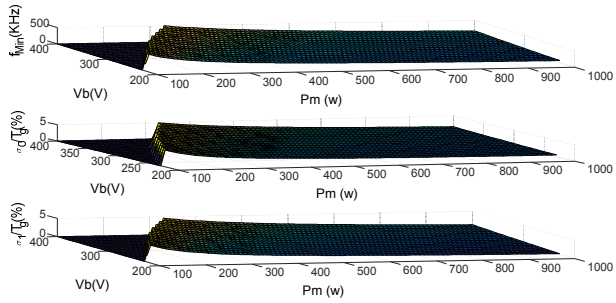

Fig. 4. Operating area of the VF-MCL-ZVS control for the designed decoupling circuit.

A and V_0 are the parameters related to the maximum power, battery voltage and decoupling

capacitor. As it is seen in (17) and (20), increasing the f_{Max} or L_d at an operating point, the window width σ decreases and vice versa. To have limited windows for σ_0 and σ_1 which is desired, L_d and f_{Max} should be chosen properly.

III. Inductor Design for Control (VF-MCL-ZVS)

The design of the decoupling inductor while operating with proposed VF-MCL-ZVS control is finding L_d so that frequency is above desired $f_{Min}{}^*$ and σ_i is small portion of line cycle for all the operating points. larger σ cause the MCL-ZVS control operate with higher loss and its performance goes away from the optimal performance. For the battery voltage or DC-link ranging from $200v - 400v$ and peak power varying from $0.1 - 1KVA$, it is desired to limit the frequency between $50 - 400KHz$ and σ_i should be less than 15% of grid period. The value of C_d is equal to $350uF$. After placing $f_{Max} = 400KHz$, f_{Min} and σ_i is plotted in Fig.3 for 4 marginal different operating points, $(400v, 1000w)$, $(400v, 100w)$ $(200v, 1000w)$ and $(200v, 100w)$ from (14), (17) and (20), as a function of L_d.

As it is seen, the operating point $(400v, 100w)$ enforce us to choose a larger inductor value to have a reduced f_{Min} and σ. This operating pint line is ignored for the design to be able to pick smaller inductor value of $L_d = 250\mu F$ which is acceptable. However, the penalty is that the converter is not operating at VF-MCL-ZVS while approaching the corner of $(400v, 100w)$. While approaching this corner, frequency is kept at $f_{Max} = 400KHz$ and ZVS is obtained with the price of higher ripple than necessary, but frequency is not going over the maximum value and an acceptable inductor is chosen. Fig.4 shows the area of operation with VF-MCL-ZVS control. In the small corner, operation is with ZVS but not with minimum conduction loss.

IV. Comparison of the Controllers

Here, a comparison between the constant frequency Continues Conduction Mode ZVS control (CCM-ZVS), proposed VF-MCL ZVS control and hard switch control for decoupling circuit is done. C_d design is shown in [9,10]. The design of the inductor for the proposed VF-MCL-ZVS control was described in the previous part of this paper. For the CCM-hard switched controlled converter, the L_d and f are kept high enough to have small ripple. A loss model considering the switching losses and conduction loss for the switches and core and copper loss for the inductor is developed and using that the loss for the decoupling circuit under three different control methods is calculated. Table I shows the design of L_d for three controls together with the loss breakdown at nominal operating point $(400v, 1Kw)$ for three control methods. It is seen that although the proposed method does not offer the smallest inductance value, its inductor is the smallest in terms of the size due to reduced peak current obtained by the controller. R_{on} of the decoupling leg switches is considered to be $200m\Omega$. Fig.5 shows the loss break down from three controls for the whole operating area. From the results, it can be seen that the proposed control, VF-MCL-ZVS control, has relatively lower losses compared to other controls.

V. Simulation and Experimental Results

Simulation results with PSIM software together with experimental results are provided to verify that the theory is correct. Simulation results for the system designed in previous part for the proposed controller and CCM-ZVS control, is shown in Fig.6 . The DC voltage is $350v$ and constant during thewhole simulation time. From the start until $t = 0.05s$, the peak power, P_m is equal to $1000VA$. As is seen, for the proposed controller (VF-MCL-ZVS) the frequency peaks when average inductor current reaches zero to limit the current ripple. Therefore, the

TABLE I. DESIGN OF L_d FOR THREE CONTROLS.

	VF-MCL-ZVS	**CCM-ZVS**	**CCM-hard switched**
$L_d(\mu H)$	100	40	450
$f(KHz)$	50-400	150	200
Total loss (w)	12.6266	148.3907	63.5762
Inductor weight (gr)	32.40	88.75	50.30
$C_d/P_m/V_b$	190µF / 0.1 – 1Kw / 100 – 400v		

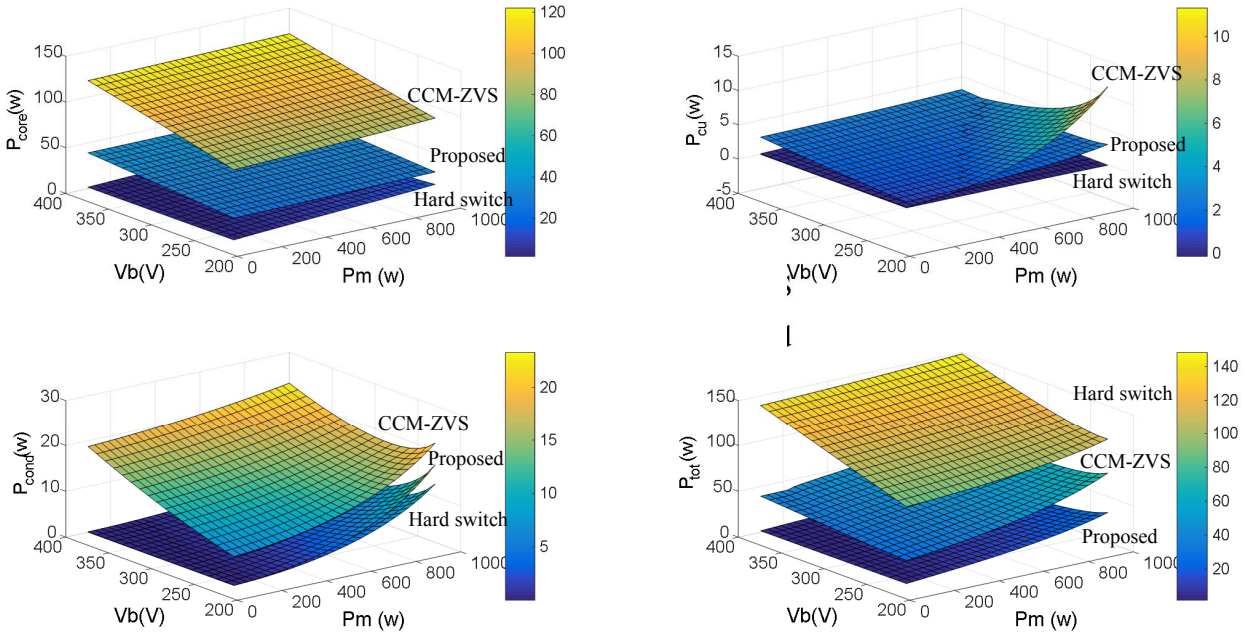

Fig. 5. Loss comparison and breakdown for three controllers over the entire operating area.

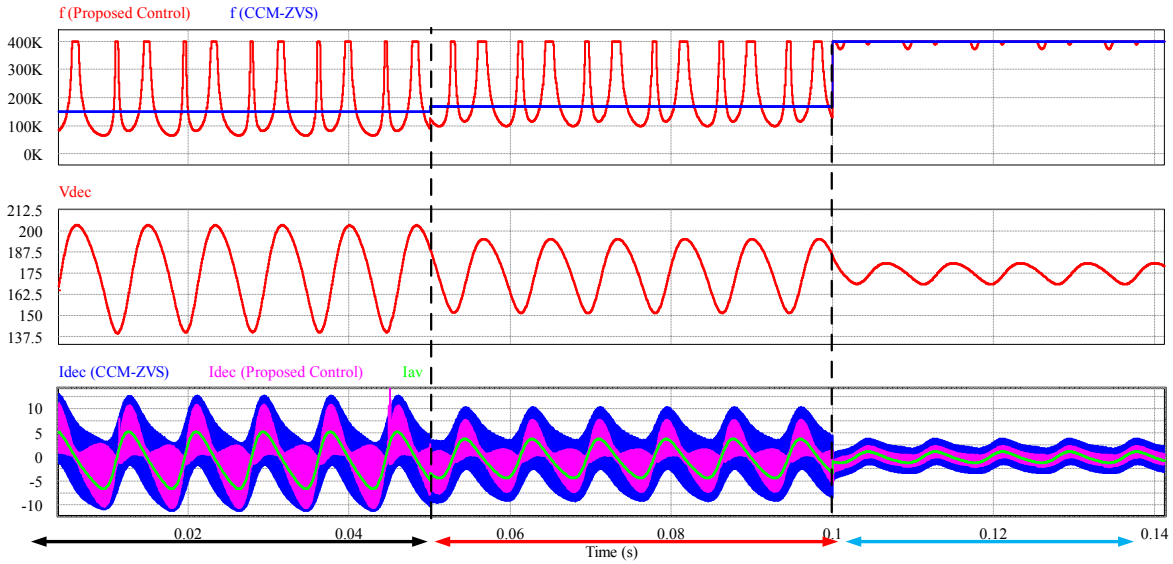

Fig. 6. VF-MCL-ZVS control for $v_{DC} = 350v$ black: $P_m = 1KVA$, red: $P_m = 700VA$ and blue: $P_m = 200VA$.

current ripple is almost always two times of the average current which is minimum possible ripple to obtain ZVS. For the CCM-ZVS control, frequency remains constant during this time window. As is seen, the proposed controller offers lower ripple compared to the CCM-ZVS controller which result is lower switch conduction and magnetic losses. At $t = 0.05s$ the peak power switch to $700VA$. As it is seen the proposed controller reduces the peak ripple current to minimize the conduction losses. The minimum frequency is higher in this time window compared to previous one. In addition, the CCM-ZVS controller increases the switching frequency and keep it constant at $f = 170KHz$ to decrease the ripple. This helps with reduction of the losses. However, during this window (0.05s-0.1s), still the proposed controller offer lower ripple. At $t = 0.1s$ P_m steps to $200VA$. As is seen, proposed controller in this mode requires higher frequency then f_{max} to shape the inductor current to have

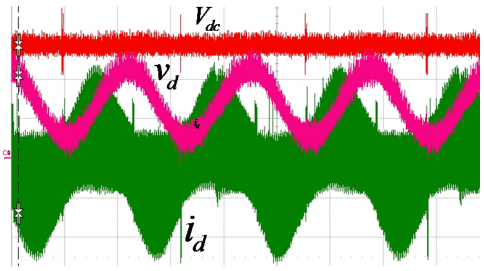

Fig. 7. VF-MCL-ZVS control: V_{dc}, v_d (20V/div), i_d (2A/div) and t (5ms/div).

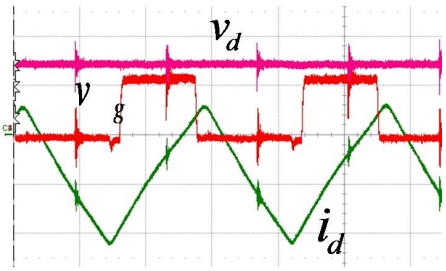

Fig. 8. VF-MCL-ZVS, switching instants: v_{gs} (10 V/div), v_d (20V/div), i_d (2A/div) and t (5μs/div)

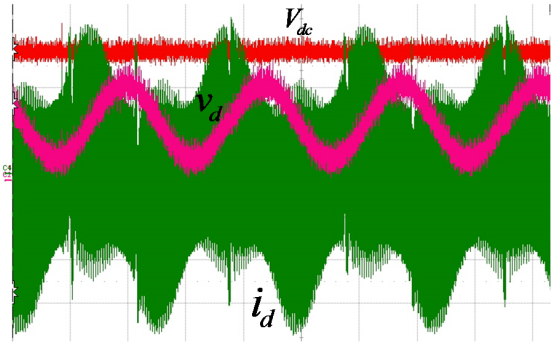

Fig. 9. CCM-ZVS control: V_{dc}, v_d (20V/div), i_d (2A/div) and t (5ms/div).

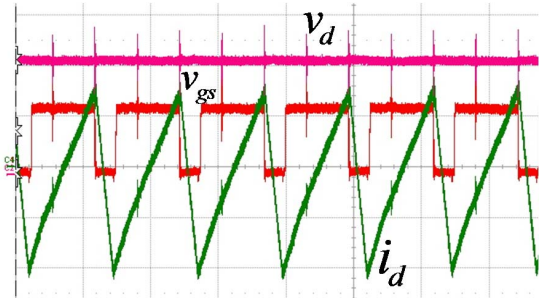

Fig. 10. CCM-ZVS control, switching instants: v_{gs}(10 V/div), v_d (20V/div), i_d (2A/div) and t (20 μs /div)

minimum current. Therefore, frequency stays close to $f_{max} = 400KHz$ or in other words, the widows $\sigma_i(i = 0,1)$ becomes very larger. While the power is transferred successfully to the decoupling capacitor and the switches operate with ZVS, extra loss due to higher ripple lower the performance in this operating point. This mode of operation is identical to the corner of the $V_b - P_m$ plane shown in Fig.4. The CCM-ZVS controller, in this time window, $(0.1 - 0.15s)$, increases the switching frequency and keep it constant $400KHz$ to limit the losses. The operation of proposed controller and CCM-ZVS controller becomes close and similar in this time window. However as it is seen, the peak current in proposed controller is a little bit smaller.

Experimental results, with the same circuit parameters, for $P_m = 200w$ and $V_{dc} = 60v$ are carried out. Digital control is implemented using a TMS320F28335 form TI. Fig.6 shows the V_{dc}, v_d and i_d for the VF-MCL-ZVS control which is the proposed control. The envelope of i_d is shaped for the two times of the average current.

Fig.7 shows the same waveform from a closer zoom. The current reaches zero and then the switch turns off. Fig.8 and Fig.9 show the same waveforms for the CCM-ZVS control. Comparison between Fig.6 and Fig.8 shows that when i_{dav} reaches zero, at the peak and valley of v_d, the proposed controller lowers the loss by increasing the frequency and decreasing the ripple and that is why the envelope of i_d is smaller in Fig.6 than that of Fig.8 . Fig.9 shows the same waveform of previous Figure but from a closer zoom. As is seen, the current goes far above zero before turning on which is producing extra loss.

VI. Conclusion

A new control method with variable switching frequency is proposed for the buck active filter operating as decoupling circuit to absorb the low frequency power produced in single-stage power conversion. the control method minimize the conduction losses through the decoupling circuit and obtains ZVS for all he switching instants. The controller is able to operate with wide range of DC voltage and power. Design and analysis are provided. A loss comparison with other available control methods are done and the results shows that the proposed control has the best performance. Simulation and experimental results are provided.

References

[1] F. Musavi, M. Craciun, D. S. Gautam, W. Eberle and W. G. Dunford, "An LLC Resonant DC–DC Converter for Wide Output Voltage Range Battery Charging Applications," in IEEE Transactions on Power Electronics, vol. 28, no. 12, pp. 5437-5445, Dec. 2013.

[2] B. Koushki, A. Safaee, P. Jain and A. Bakhshai, “Review and comparison of bi-directional AC-DC converters with V2G capability for on-board EV and HEV,” IEEE Transportation Electrification Conference and Expo (ITEC) 2014, vol., no., pp.1,6, 15-18 June 2014.K. Elissa, “Title of paper if known,” unpublished.

[3] S. Li, J. Deng and C. C. Mi, "Single-Stage Resonant Battery Charger With Inherent Power Factor Correction for Electric Vehicles," in *IEEE Transactions on Vehicular Technology*, vol. 62, no. 9, pp. 4336-4344, Nov. 2013.

[4] M. Jang, M. Ciobotaru and V. G. Agelidis, "A Single-Stage Fuel Cell Energy System Based on a Buck--Boost Inverter with a Backup Energy Storage Unit," in IEEE Transactions on Power Electronics, vol. 27, no. 6, pp. 2825-2834, June 2012.

[5] Y. Sun, Y. Liu, M. Su, W. Xiong and J. Yang, "Review of Active Power Decoupling Topologies in Single-Phase Systems," in IEEE Transactions on Power Electronics, vol. 31, no. 7, pp. 4778-4794, July 2016.

[6] H.L.Chan, "A new battery model for use with battery energy storage systems and electric vehicles power systems," Power Engineering Society Winter Meeting, 2000. IEEE, vol.1, no., pp.470,475 vol.1, 2000.

[7] Feng Gao, Ding Li, P. C. Loh, Yi Tang and Peng Wang, "Indirect dc-link voltage control of two-stage single-phase PV inverter," 2009 IEEE Energy Conversion Congress and Exposition, San Jose, CA, 2009, pp. 1166-1172.

[8] A. K. Verma, B. Singh and D. T. Shahani, "Vehicle to grid and grid to vehicle bidirectional power flow at unity power factor with DC ripple compensation," 2012 IEEE 7th International Conference on Industrial and Information Systems (ICIIS), Chennai, 2012, pp. 1-6.

[9] B. Kouski, P. Jain and A. Bakhshai, "Half-bridge full-bridge AC-DC resonant converter for bi-directional EV charger," 2017 IEEE Applied Power Electronics Conference and Exposition (APEC), Tampa, FL, 2017, pp. 3681-3687.

[10] B. Koushki, P. Jain and A. Bakhshai, “A Bidirectional AC-DC Converter for Electric Vehicle with No Electrolytic Capacitor,” 2016 IEEE 7th International Symposium on Power Electronics for Distributed Generation Systems (PEDG), Vancouver, 2016, pp.

[11] R. Wang et al., "A High Power Density Single-Phase PWM Rectifier With Active Ripple Energy Storage," in IEEE Transactions on Power Electronics, vol. 26, no. 5, pp. 1430-1443, May 2011.

[12] X. Cao, Q. C. Zhong and W. L. Ming, "Ripple Eliminator to Smooth DC-Bus Voltage and Reduce the Total Capacitance Required," in IEEE Transactions on Industrial Electronics, vol. 62, no. 4, pp. 2224-2235, April 2015.

[13] J. Kolar U. Drofenik J. Biela M. Heldwein H. Ertl T. Friedli and S. Round "PWM converter power density barriers " IEEJ Trans. IA vol. 128 no. 4 pp. 1-14 2008.

[14] H. Wang, S. Dusmez and A. Khaligh, "Maximum Efficiency Point Tracking Technique for LLC-Based PEV Chargers Through Variable DC Link Control," in IEEE Transactions on Industrial Electronics, vol. 61, no. 11, pp. 6041-6049, Nov. 2014.